JOURNAL OF GEOPHYSICAL RESEARCH, VOL. 106, NO. C5, PAGES 9327–9338, MAY 15, 2001

Comparison between predicted and observed sand waves and sand banks in the North Sea

Suzanne J. M. H. Hulscher and G. Matthijs van den Brink
Department of Civil Engineering, University of Twente, Enschede, Netherlands

Abstract. For the first time a prediction model of regular morphological patterns on the seabed was tested against observations of sand wave and sand bank occurrence in the entire North Sea. The model, which originates from first physical principles, predicts this occurrence via two dimensionless parameters on the basis of the water depth, the tidal velocity amplitude, the level of zero intercept above the seabed (z_0), and a viscosity variation parameter ε. The latter two quantities were varied in a number of predictions for the entire North Sea, whereas for the first two, local values were used. The range of realistic values of ε and z_0 was large enough to let these two parameters distinguish between the possible (combinations of) bed forms, as is shown in the shallower southern bight of the North Sea. The results were more sensitive to variations in z_0 than in ε. A slightly more detailed approach focused on sand waves only in the southern North Sea and estimated local values for z_0 using depth information. Quantification of the results showed that the model was able to predict the contours of the sand wave patches, but it could not account for the absence of the bed features within this area. The type of bed deposit partly explains the smaller-scale variation. The work confirms the validity of the theoretical bed form prediction model and verifies the hypothesis that the large-scale seabed features are formed as free instabilities of tide-topography interactions.

1. Introduction

The bottom of many shallow seas is not flat; it exhibits regular patterns at various spatial scales. These submarine patterns appear in patches that may overlay each other. In this paper only the large-scale patterns are considered, i.e., tidal sand banks and sand waves. Knowledge about tidal sand banks and sand waves is relevant to various practical problems related to the coast and the seabed [cf. *Whitehouse et al*., 1998; *Langhorne*, 1978]. Coastlines, for example, in front of which tidal sand banks are located, seem to suffer less from heavy storms. Pipelines and cables crossing a sand wave field may become exposed, and even free spans may occur. Also, navigation channels, for example "Eurogeul" near the port of Rotterdam, suffer from the existence of sand waves as these bed features migrate into the channel. For reasons of safety and economics, pipelines are now trenched deep into the seabed, and navigation channels are continuously dredged. A better knowledge of sand waves may prepare the way for substantial savings for pipeline construction and dredging.

Tidal sand banks and sand waves have in common that they are approximately harmonic in one horizontal direction and are elongated perpendicular to this direction. Tidal sand banks have wavelengths of about 5 km and amplitudes of up to 40 m. Sand waves are smaller in wavelength ($\pm$500 m) and amplitude (about 5 m). A further difference between the two patterns is the orientation with respect to the mean tidal current: tidal sand bank crests are oriented about 30° cyclonically with respect to the main axis of the prevailing tidal current; sand waves are more or less perpendicular to this axis.

Huthnance [1982] advanced the idea that tidal sand banks are generated by interactions of the tidal motion and the sandy sea bed. He used a morphodynamic model based on a simplified description of the two-dimensional depth-averaged tidal motion, conservation of sediment, and a bed load sediment transport parameterization. The fastest growing free unstable modes in this model correspond to tidal sand banks. This conclusion was confirmed analytically by the work of *Hulscher et al*. [1993].

Hulscher [1996] extended this idea by modeling the tidal motion in three dimensions. Thus the vertical structure of the tidal flow is represented, including circulations in the vertical plane. This three-dimensional model shows that in addition to tidal sand banks, sand wave-like patterns are generated. On the basis of the vertical structure of the tidal motion four types of bed behavior may occur: tidal sand banks only, sand waves only, both patterns combined, or a flat sea bed.

The vertical structure of the tidal motion and the shear stress it exerts on the bed are characterized by two parameters, E_v (Stokes number) and $\hat{S}$ (resistance parameter). These parameters are not directly known from measurements. In order to provide estimates for these two parameters this paper proposes an analogy between two turbulence models: (1) a simple model based on E_v and $\hat{S}$ and (2) a slightly more sophisticated turbulence model based on the level of zero intercept z_0, the height above the bed at which the velocity drops to zero, in combination with a parabolic turbulent viscosity in which the parabolic shape depends on the parameter ε, such that the ratio between the multipliers of quadratic term and linear term in z is ε/H.

Hence, on the basis of theory alone, there is a model for predicting the occurrence of large-scale bed form patterns in a shallow sea. The main subject of this paper is to investigate the validity of this model by testing it against observations in the North Sea. In order to perform such a comparison the same

Paper number 2001JC900003.
0148-0227/01/2001JC900003$09.00

level of aggregation of the data and the predictions has to be chosen. This means that when testing on the occurrence of different types of bed forms, the treatment must be chosen such that horizontal differences are expressed in an appropriate way. This paper uses two such levels of aggregation. The first is used for testing whether or not the model is able to discriminate between presence or absence of a certain class of bed forms. The second, more detailed level of aggregation, attempts to quantify the validity of the prediction for one type of pattern, i.e., sand waves.

The paper is organized as follows. Section 2 describes the observed occurrence of rhythmical bed features in the North Sea on the basis of several sources in the literature. Section 3 briefly describes the Geographical Information System that has been used to produce the results presented in this paper. Section 4 outlines the bed form prediction model as well as methods to apply this model to the North Sea. Section 5 presents and discusses the results of a first attempt to predict bed features in the North Sea using constant values for some model parameters. Section 6 focuses attention on the sand waves in the southern part of the studied area; local estimates are found for the level of zero intercept, z_0. Section 7 summarizes the conclusions.

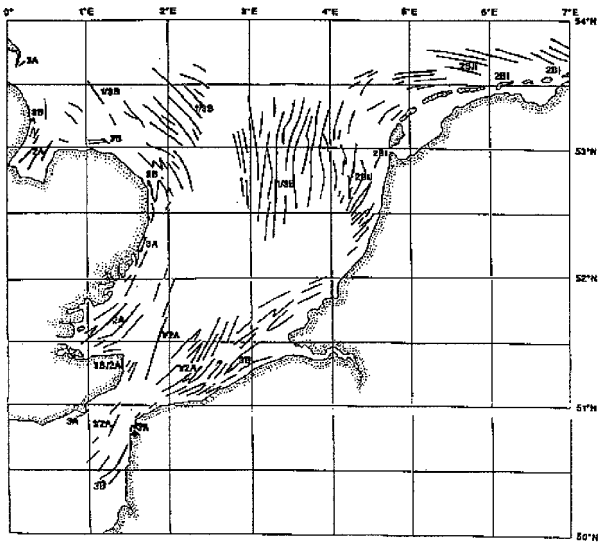

Figure 1. Locations of several tidal sand bank Systems in the North Sea [from *Dyer and Huntley*, 1999].

2. Occurrence of Rhythmical Bed Features in the North Sea

A detailed description of the occurrence of tidal sand banks and sand waves requires synoptic information within the study area. Such synoptic surveys have not been performed systematically in the North Sea.

The most detailed information about sand wave occurrence in the North Sea is furnished by the geological charts issued by the British, Dutch, and Belgian Geological Services [*Rijks Geologische Dienst*, 1984; *Hydrographer of the Navy*, 1992]. These charts cover the area between 51° and 54°N and from the British coast to 4°E. Therefore these data must be combined with other sources to gain information over a larger area and for sand waves and tidal sand banks. *Van Alphen and Damoiseaux* [1989] present observations of both tidal sand banks and sand waves along the Dutch coast. Their observations of tidal sand banks link in with the review of *Dyer and Huntley* [1999] (see Figure 1). The sand wave data of *Van Alphen and Damoiseaux* [1989] are used in addition to the geological charts. The result is shown in Figure 2, a map of sand wave occurrence in the region of the North Sea between the 51° and 54°N.

Information about sand wave occurrence north of 54°N is scarce. *Stride* [1982] submits the idea that the southern bight of the North Sea is almost completely covered with sand waves (Figure 3). This is not generally accepted and contradicts other sources, for example, the geological charts in Figure 2. Nevertheless, Figure 3 will be used to indicate where sand waves can be expected north of 54°N.

3. Geographical Information System of the North Sea

The objective of a Geographical Information System (GIS) is to connect any kind of information to a (digital) land or sea chart for any location or area. The system described here contains information about the North Sea between the line Dover-Calais and the latitude 57°N. The data are held on a rectangular grid at a spatial resolution of 500 m in either horizontal direction. There is hardly any source of information that covers the entire area. In this study the GIS is used in two ways. The first is to combine information about sand waves. This enables the investigation of direct correlations between sand wave features and, for example, tidal components, wind wave data, or grain size distribution [see *Bijker et al*., 1998]. The second way is to use the information in the system as input to the bed features prediction model, thus enabling predictions of bed patterns in the North Sea.

The information system contains sand wave data (occurrence (see Figure 2), maximum sand wave height, and orientation) and related data. The latter include the water depth, the median grain size of the sand fraction, the distribution of bed deposits (sand, gravel, and mud) over the sea bed, and the tidal data for the components M_0, M_2, and M_4 (water level amplitude, long axis of the tidal ellipse, and inclination of the long axis).

Information about the median grain size of the sand fraction and the spatial distribution of bed deposits is obtained from *Rijks Geologische Dienst* [1984] and *Hydrographer of the Navy* [1992]. Bathymetry and tidal data are obtained from calibrated

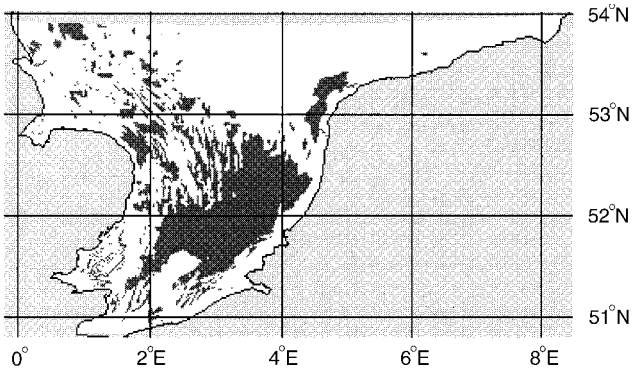

Figure 2. Observed sand waves in the Southern North Sea [from *Rijks Geologische Dienst*, 1984; *Hydrographer of the Navy*, 1992; *Van Alphen and Damoiseaux*, 1989].

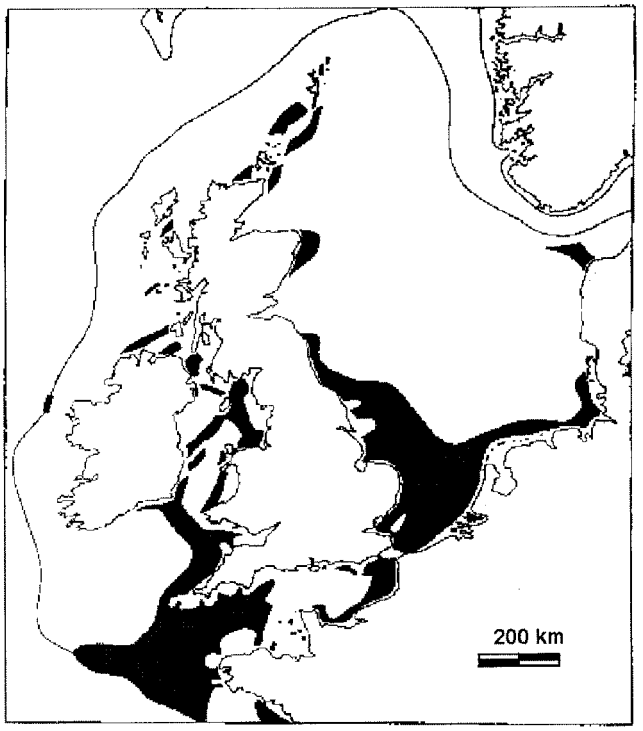

Figure 3. Locations of sand waves having amplitudes larger than 1.5 m, around the British Isles [from *Stride*, 1982]. This map covers the area between 47° and 60°N and 10°W and 10°E.

numerical models [*Boon and Gerritsen*, 1997; *Ten Brummelhuis et al*., 1997; *Van Dijk and Plieger*, 1988].

In many cases the level of accuracy of the data is unknown. However, since this study aims to provide a first insight into the morphodynamic system and does not result in detailed predictions, the level of accuracy is assumed to be sufficient.

Figure 4 shows an example of the type of information to be derived from the GIS and relates the bed composition (see Table 1) to the occurrence of sand waves. The white stacks indicate the distribution of bed material over the largest area for which bed type information is available. The shaded stacks constitute the same distribution but now restricted to the areas that are covered with sand waves (26% of the first area). Differences in these two distributions indicate differences in bed material composition between sand wave areas and the entire area.

Table 1. Explanation of Codes From Geological Charts

Code	Description	Ratio Sand:Mud	Percent of Gravel
G	gravel		>80
msG	muddy sandy gravel	1:1–9:1	30–80
sG	sandy gravel	>9:1	30–80
gS	gravelly sand	>9:1	5–30
(g)S	slightly gravelly sand	>9:1	1–5
S	sand	>9:1	<1
mS	muddy sand	1:1–9:1	<1
sM	sandy mud	1:9–1:1	<1

Figure 4 also indicates that sand waves in the North Sea occur almost exclusively in sandy beds. This is in good agreement with the literature [see *Fenster et al*., 1990; *Terwindt*, 1971]. Sand waves have a preference for sand (<1% gravel) and slightly gravelly sand (1–5% gravel). In gravelly sand (5–30% gravel), sand waves do occur, but they cover only a small percentage of the area. Most sand waves occur at locations where the bed consists of pure sand. At places where moderate to large amounts of gravel or mud are found, sand waves are not observed.

4. Bed Features Prediction Model

The hypothesis underlying the morphological model of *Hulscher* [1996] is that large-scale bed form patterns are free instabilities of the morphodynamic system, i.e., the coupled system of water and sediment motion and bed evolution. The model is based on the three-dimensional shallow water equations applied to tidal flows. The sediment transport is modeled using a bed load transport formula extended to include a downhill gravitational component:

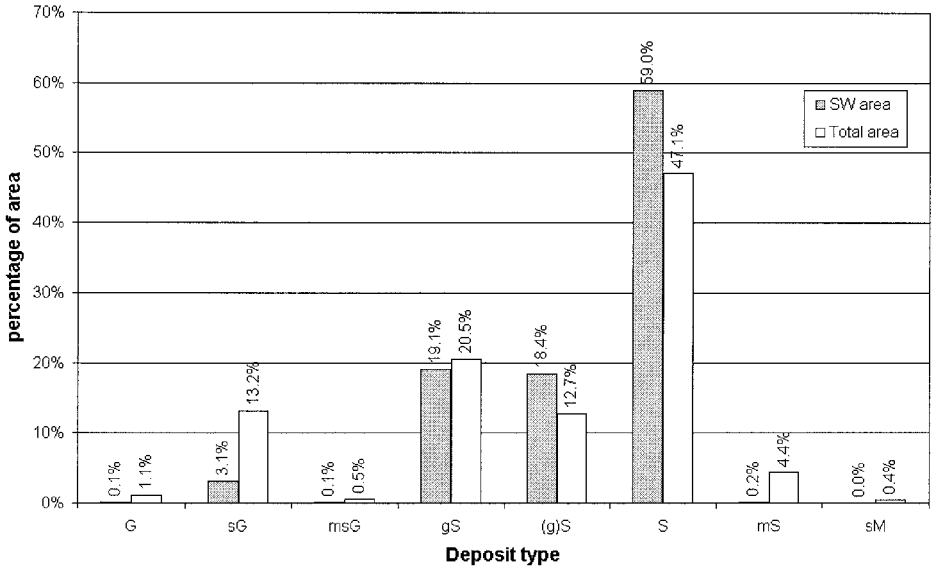

Figure 4. Distribution of bed material over sand wave and total area.

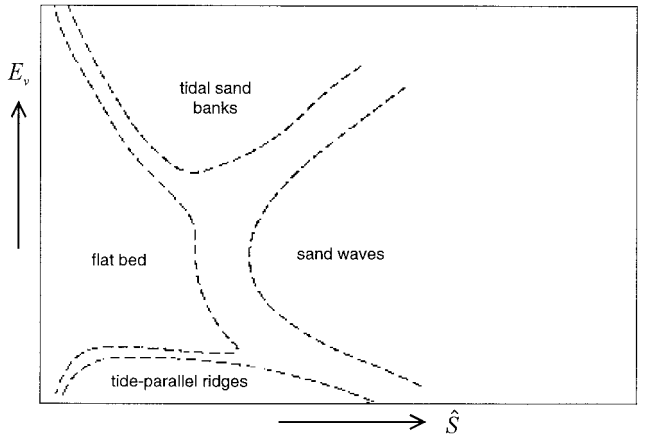

Figure 5. Characteristic bed forms predicted by the three-dimensional shallow water model as a function of the resistance parameter $\hat{S}$ and the Stokes number E_v [*Hulscher*, 1996].

$$\mathbf{Q} = [|\boldsymbol{\tau}_b|]^p \left\{ \frac{\boldsymbol{\tau}_b}{|\boldsymbol{\tau}_b|} - \lambda \nabla h \right\}. \tag{1}$$

Bed level changes are computed from the sediment balance equation. The horizontal boundaries are assumed to be infinitely far away, thus making it possible to select harmonic boundary conditions. This essentially nonlinear model is, after linearization for small perturbations, subject to a linear stability analysis (harmonic mode analysis). Starting from a flat bed, the fastest growing harmonic mode in the bottom topography is identified. For different values of the parameters E_v (the Stokes number) and $\hat{S}$ (the resistance parameter), different dominant modes are found, which can be identified as tidal sand banks, sand waves, tide parallel ridges, or flat beds (Figure 5).

The parameters E_v and $\hat{S}$ are defined as

$$E_v = \frac{2A_v}{\sigma H^2} \qquad \hat{S} = \frac{2S}{\sigma H}, \tag{2}$$

in which H is the local mean depth and σ is the frequency of the tidal motion. The eddy viscosity A_v ($m^2\ s^{-1}$) is taken as a constant, i.e., independent of the vertical coordinate. This implies that a partial slip condition has to be applied at the bed. Here a linear relation between the slip velocity at the bed and the bed shear stress is adopted; the dimensional quantity S ($m\ s^{-1}$) quantifies their ratio. This partial slip approach overcomes the problem that a constant eddy viscosity model with a no-slip condition at the bed near the bottom is unable to reproduce realistically both the velocity and the shear stress. The constants A_v and S are considered to describe the vertical profile of the horizontal flow components in uniform shear flow [after *Engelund*, 1970].

Since the Stokes number and the resistance parameter cannot be measured directly, a method must be derived to estimate these parameters from the available data. To that end, simplified horizontally uniform tidal flow is considered. The two parameters E_v and $\hat{S}$ are estimated by fitting the partial slip model, described above, to a more realistic turbulence model characterized by a no-slip condition near the bed and a parabolic eddy viscosity:

$$\nu_t = \kappa \hat{u}_* z \left(1 - \varepsilon \frac{z}{H}\right), \tag{3}$$

in which κ is the Von Karman constant. This parabolic viscosity profile includes the parameter ε, which may range from 0.5 (maximum viscosity at the water surface) to 1.0 (zero viscosity at the water surface; maximum viscosity halfway up the water column). In addition, the bed boundary condition is based on the prescription of the level of zero intercept meaning that the velocity $\tilde{u}$ equals zero at a prescribed level z_0 just above the sea bed:

$$\tilde{u} = 0 \qquad z = z_0. \tag{4}$$

The criteria to fit the constant eddy-viscosity/partial slip model to the more realistic model are that both models have the same water discharge and depth-averaged viscosity.

The procedure to find expressions for E_v and $\hat{S}$ can be found in Appendix A. It yields the following expressions:

$$E_v = \frac{\kappa^2 B}{A} \frac{3\pi}{4} \frac{u_m}{H\sigma} \qquad \hat{S} = \frac{\kappa^2 B}{A(AB - \frac{1}{3})} \frac{3\pi}{4} \frac{u_m}{\sigma H}, \tag{5}$$

in which u_m is the depth-averaged velocity amplitude at a particular location. Furthermore,

$$A = \left[\ln\left(\frac{H}{z_0}\right) - \frac{1}{\varepsilon} + \frac{1-\varepsilon}{\varepsilon} \ln\left(\frac{1-\varepsilon}{1-\varepsilon\frac{z_0}{H}}\right) + \frac{\varepsilon - 1}{\varepsilon^2} \ln(1-\varepsilon) \right] \qquad B = \frac{3-2\varepsilon}{6}. \tag{6}$$

Thus four input parameters are required to find local values for these parameters: u_m (depth-averaged flow velocity), H (water depth), ε (viscosity variation parameter), and z_0 (level of zero intercept).

So, rather than two parameters that are not directly measurable, this new formulation of the problem has led to four parameters. Two of them, z_0 and ε, are still not readily measurable. However, these parameters are easier to estimate than the Stokes number and the resistance parameter.

5. Prediction of Bed Forms in the Entire North Sea

At a fixed location, with a given depth H and a tidal velocity u, the values of E_v and $\hat{S}$ depend on z_0 and ε. Since these parameters are functions of, for example, grain size, bed composition, small-scale bed forms, and swell, it seems obvious that these parameters are far from homogeneous throughout the North Sea. However, detailed knowledge about the processes involved and their subsequent distribution is not available. Hence, by way of a first step, horizontally uniform values of ε and z_0 are used to make the predictions.

To be able to provide bed pattern estimates, the qualitative figure by *Hulscher* [1996], Figure 5, is quantified in Figure 6. For this quantification a characteristic parameter setting for the North Sea is used: Coriolis parameter, $f = 1.16 \times 10^{-4}\ s^{-1}$; the frequency of the M_2 tidal component, $\sigma = 1.4 \times 10^{-4}\ s^{-1}$; the exponent p in the bed load sediment transport equation (1), $p = 1.5$; the downhill gravitational transport coefficient in (1): $\lambda = 2.0$; and water depth, $H = 30$ m. Note that the depth H is used in two different ways. One general value has been used to construct Figure 6. To use Figure 6 in the predictions, E_v and $\hat{S}$ are estimated locally by using the local

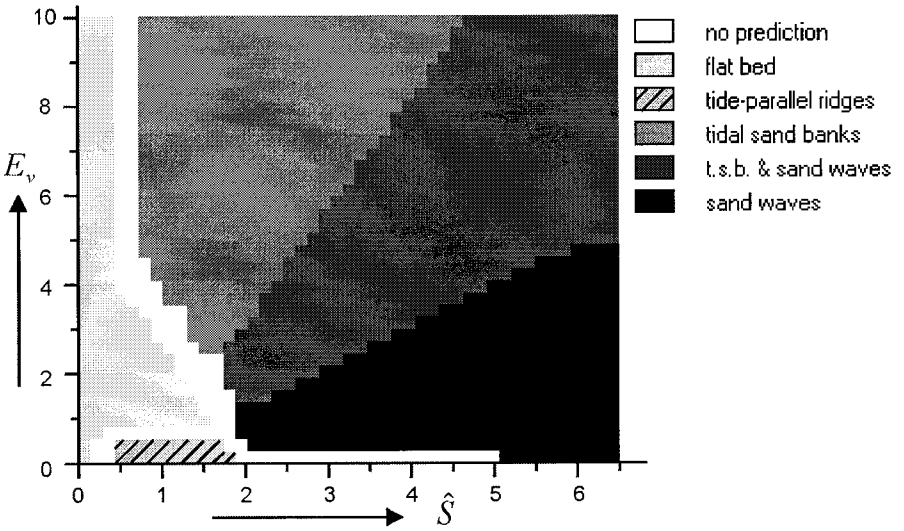

Figure 6. Quantification of Figure 5: predicted bed pattern as a function of E_v and $\hat{S}$.

depth. These two approaches are not contrary as long as the parameters E_v and $\hat{S}$ depend on at least two independent parameters other than the local depth. In section 4 this has been shown to be the case.

In between the flat bed and the various bed patterns, there is a transition zone in which wavelength, orientation, and growth rate change strongly, so that the actual bed pattern cannot be linked uniquely to one of the physical states. In order to avoid this unclarity these boundaries have been given a certain width, resulting in an undefined bed state: here the result is that the model does not provide a prediction. Furthermore, combinations of E_v and $\hat{S}$ beyond the parameter combinations shown in Figure 6 yield no prediction either. In addition to the bed forms in Figure 5, the sand wave domain is divided into two parameter regions: one in which sand waves are the only unstable large-scale bed pattern and one in which sand waves and tidal sand banks coexist (and sand waves are growing fastest according to Figure 5). This addition has been made to account for the joint occurrence of the two bed forms, reported in the literature [*Huntley et al*., 1993; *Van Alphen and Damoiseaux*, 1989]. It also complies with the model since *Hulscher* [1996] found asymmetric contour plots for these parameter combinations, indicating that both tidal sand banks and sand waves are initially unstable. For sand waves the crests are nearly perpendicular with respect to the tidal motion, so that the contour plots for the unstable large modes are (almost) symmetrical [see *Hulscher*, 1996, Figure 7a]. For sand banks we have a significant counterclockwise crest orientation with respect to the tidal motion, showing an asymmetric contour plot [see *Hulscher*, 1996, Figure 5a] for the unstable, small modes. So, when sand waves are most unstable and we find an (sand bank) asymmetry in the small-mode region, we expect both features to develop. However, when this sand bank asymmetry is absent, we expect only sand waves to develop. The criteria we used to discriminate here is that for asymmetry the line connecting the zero and the fastest growing modes (i.e., the sand wave mode) has to be over 50% wider for counterclockwise modes and have a spacing larger than 3.6 km.

The theoretical model of *Hulscher* [1996] predicted a pattern she called "tide-parallel ridges." They have the same spatial and temporal scales as tidal sand banks, but their crests' orientation is parallel to the prevailing tidal current. The main reason for their inclusion here is to find out where this theoretically encountered pattern is to be expected in the North Sea.

To provide estimates for the Stokes number and the resistance parameter, the local depth and the local amplitude of the tidal velocity are required as input. The latter parameter is digitized from a chart by the *Directorate of Fisheries* [1981] (Figure 7); the former is provided on a nonregular grid, as described by *Boon and Gerritsen* [1997] and *Ten Brummelhuis et al*. [1997] (see Figure 8).

The combinations of the parameters ε and z_0 used in this section are given in Table 2. If small values for the level of zero intercept z_0 are chosen, the value of the resistance parameter is relatively small in the entire North Sea. Therefore sand wave generation is not to be expected. If the smallest possible value of the viscosity parameter ε is chosen, the Stokes parameter and the resistance parameter are large, thus favoring the formation of tidal sand banks. The prediction for this combination

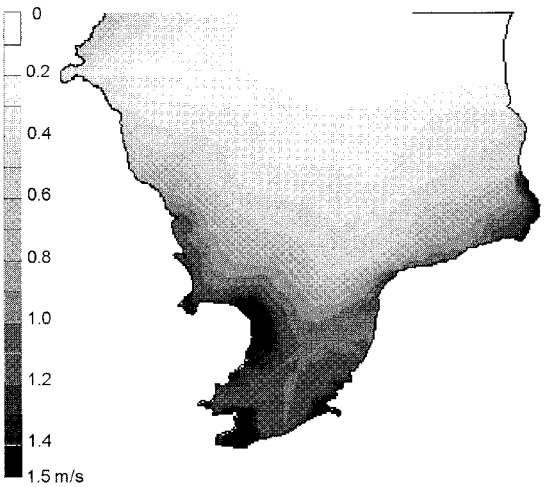

Figure 7. Depth-averaged M_2 tidal velocity amplitude [*Directorate of Fisheries*, 1981]; values range from 0 to 1.5 m s^{-1}.

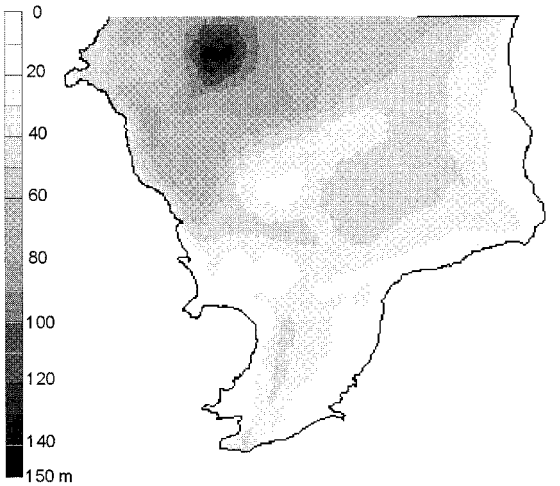

Figure 8. Bathymetry of the North Sea [*Boon and Gerritsen*, 1997; *Ten Brummelhuis et al*., 1997]; values range from 0 to 150 m.

($z_0 = 10^{-5}$ m and $\varepsilon = 0.5$) is shown in Figure 9. Most of the North Sea bed is predicted to be flat, and only in some patches near the coastlines are tidal sand banks predicted. Other bed forms are not predicted, implying that in the case of very small roughness at a certain location a flat bed will probably occur.

Comparison with Figures 1, 2, and 3 shows that the situation described in Figure 9 does not comply with the observation of both tidal sand banks and sand waves in the southern part of the North Sea. However, for the northern part of the study area, Figure 9 agrees with the observations.

By keeping the viscosity parameter fixed while increasing the roughness, the region in the prediction scheme that contains combinations of the parameters E_v and $\hat{S}$ predicting the generation of tidal sand banks will extend to greater depths, and hence the total area of tidal sand bank occurrence is expected to increase. The result for such a parameter setting ($\varepsilon = 0.5$ and $z_0 = 10^{-3}$ m) is shown in Figure 10. As expected, the area for which the model predicts tidal sand banks has increased, leading to the conclusion that an intermediate roughness at a certain location favors the formation of tidal sand banks.

Comparison with Figure 1 shows that the area where tidal sand banks are predicted has a similar shape to the area where they are observed, but the predicted area is smaller. Still, no sand waves have been predicted. From these results one can conclude that at the same locations the bed roughness, i.e., the level of zero intercept z_0, can make the difference between a flat bed and tidal sand banks.

Keeping the viscosity parameter fixed and increasing the roughness parameter further to $z_0 = 10^{-2}$ m produces Figure 11. The darker shades near the coastlines indicate the coexistence of sand waves and tidal sand banks. Note that for a smaller z_0 the model predicts tidal sand banks only. Furthermore, large areas up north have become white, implying that the model does not predict either a flat bed or any other bed form.

Table 2. Combination of Parameters z_0 and ε for Which Predictions are Discussed in Section 5

	z_0			
ε	10^{-5} m	10^{-3} m	10^{-2} m	10^{-1} m
0.5	Figure 9	Figure 10	Figure 11	Figure 12
0.99			Figure 13	Figure 14

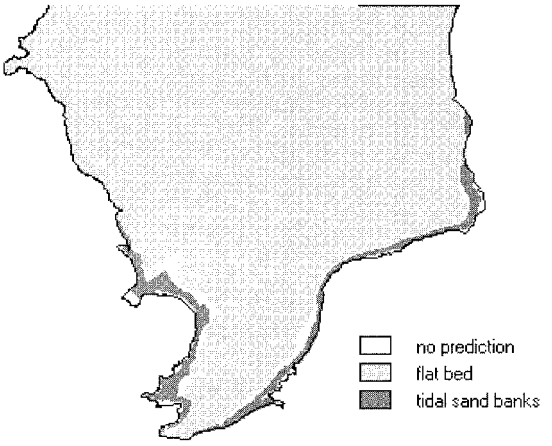

Figure 9. Predictions based on the diagram shown in Figure 6 in the case of overall North Sea values $\varepsilon = 0.5$ and $z_0 = 10^{-5}$ m.

According to Figure 1 the area where tidal sand banks are predicted is fairly large. This parameter setting also yields sand wave predictions near the coasts, but from Figure 2 it can be observed that sand waves are also present at locations for which no sand wave prediction is given in Figure 11.

Increasing the level of zero intercept to a very high value, $z_0 = 10^{-1}$ m, still keeping ε at 0.5, results in the prediction given in Figure 12. Patches of sand banks alone are not found anymore; the only two remaining predictions are "flat bed" and "sand banks and sand waves." The main area in which to expect bed features has shifted from the southern to the central part of the North Sea. Along the coasts of the continent and Great Britain a relatively large strip is found where E_v and $\hat{S}$ reach values that exceed the upper boundary of the range of these parameters in the prediction scheme, so no prediction is given.

Comparing Figure 12 with the observations in Figures 1 and 2 shows that for both types of bed features the predictions are

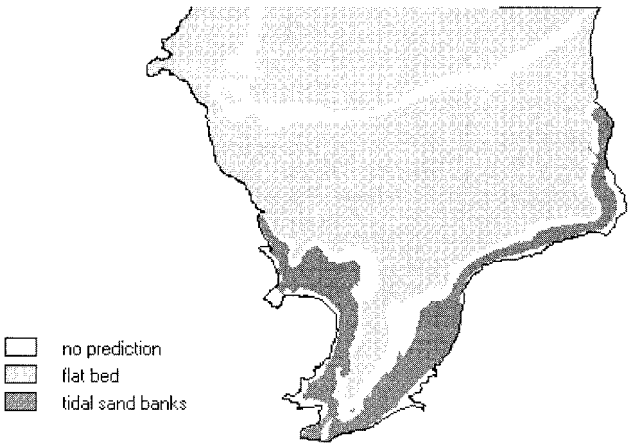

Figure 10. Predictions based on the diagram shown in Figure 6 in the case of overall North Sea values $\varepsilon = 0.5$ and $z_0 = 10^{-3}$ m.

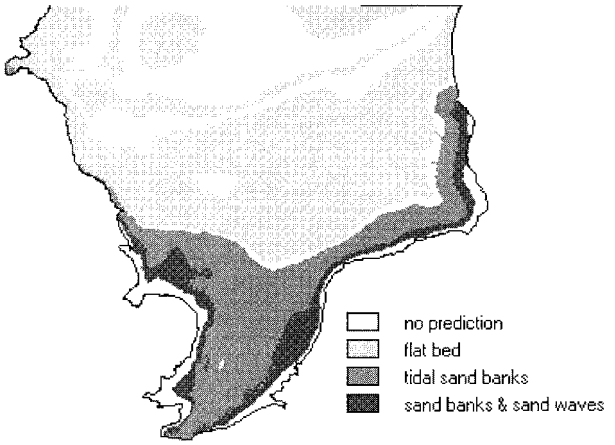

Figure 11. Predictions based on the diagram shown in Figure 6 in the case of overall North Sea values $\varepsilon = 0.5$ and $z_0 = 10^{-2}$ m.

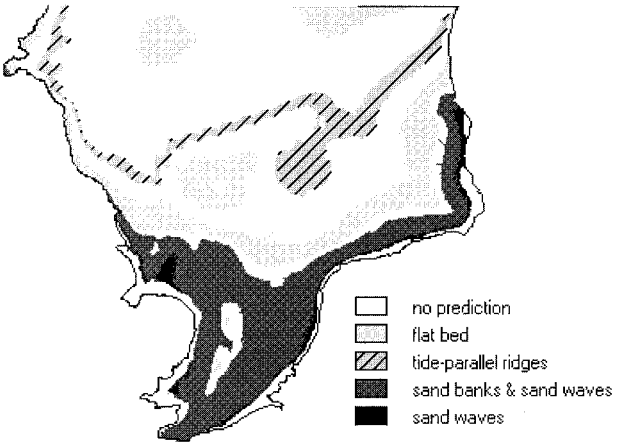

Figure 13. Predictions based on the diagram shown in Figure 6 in the case of overall North Sea values $\varepsilon = 0.99$ and $z_0 = 10^{-2}$ m.

not very realistic: the predicted sand wave areas are located too far north and too far off the coasts. From these results it can be concluded that at some locations the level of zero intercept z_0 can make the difference between a flat bed, tidal sand banks, and a combination of tidal sand banks and sand waves.

To show the effects of the variation of the viscosity parameter on the predicted bed patterns, the value of ε has been varied between its minimum 0.5 and its practical maximum 0.99, keeping the level of zero intercept constant at $z_0 = 10^{-2}$ m and $z_0 = 10^{-1}$ m, respectively. The theoretical maximum of ε, i.e., 1.0 (see section 4), has not been used since this value causes computational problems.

From Figure 6 it can be seen that a large value of ε favors the prediction of sand waves rather than tidal sand banks since the Stokes number E_v turns out to decrease with increasing ε on the present domain of interest (see (5)–(6)). Another consequence of this relation between E_v and ε is that fewer locations will have a flat bed prediction and more locations will have no prediction given. Also, the prediction of tide parallel ridges may be expected when the Stokes number becomes very small.

Figure 13 shows the prediction for $z_0 = 10^{-2}$ m and $\varepsilon = 0.99$. As expected, for many locations no prediction has been made, whereas some locations in the northern part of the study area have an indication of tide parallel ridges. Comparing Figure 13 with Figure 11 shows that the prediction has shifted from mainly sand banks to a combination of sand banks and sand waves. The area with only tidal sand banks has vanished. Also, along the coasts some locations can be observed with a sand waves only indication (the dark areas). In the southern part, there are two small areas for which a flat bed is predicted. There are no patches for which only tidal sand banks are predicted. The predicted flat bed in the southern part complies with the observations in Figure 1. The prediction of sand waves near the British coast is not very realistic, according to Figure 2, in which it can be observed that sand wave patches become very scattered in these locations.

The prediction in Figure 14 is based on the parameter combination $z_0 = 10^{-1}$ m and $\varepsilon = 0.99$. Comparing Figure 14 with Figure 12, it can be observed that locations for which Figure 12 showed a combination of sand waves and sand banks now have a sand wave only prediction. There are hardly any locations for which a flat bed has been predicted, whereas tide parallel ridges are expected in a large area. The fact that no tidal sand banks are predicted does not comply with the observations.

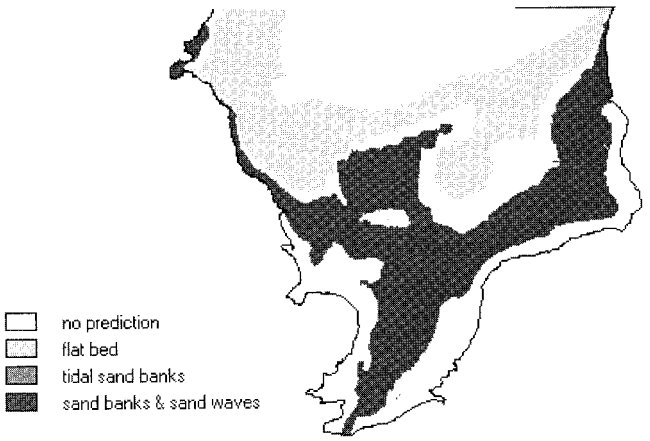

Figure 12. Predictions based on the diagram shown in Figure 6 in the case of overall North Sea values $\varepsilon = 0.5$ and $z_0 = 10^{-1}$ m.

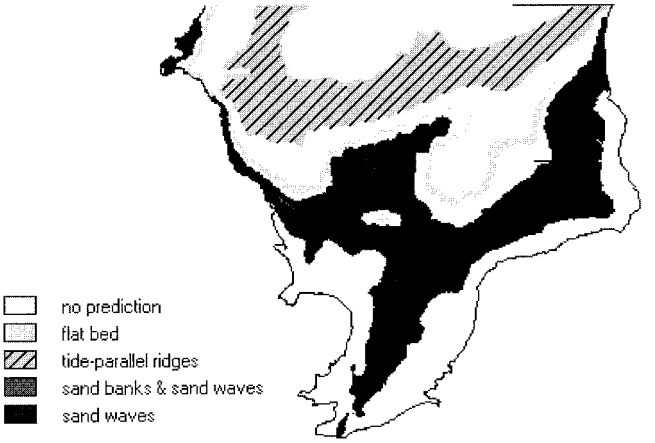

Figure 14. Predictions based on the diagram shown in Figure 6 in the case of overall North Sea values $\varepsilon = 0.99$ and $z_0 = 10^{-1}$ m.

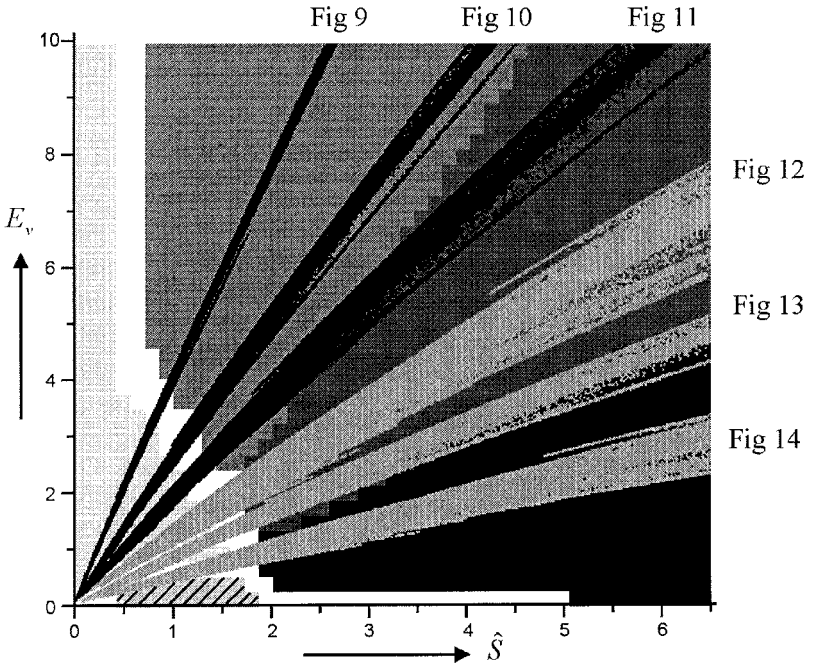

Figure 15. Calculated parameter combinations in the prediction scheme for Figures 9–14. For parameter settings, refer to Table 2.

Also, no sand waves are observed as far north as is predicted in Figure 14, while they are known to be much closer to the coasts than predicted.

Figure 15 shows the calculated values of E_v and $\hat{S}$ leading to the predictions in Figures 9–14. As a reference, the prediction scheme of Figure 6 is shown in the background. It shows that the ranges of ε and z_0 values used cover most of the possible $(E_v, \hat{S})$ combinations; that is, the entire prediction scheme is used. A combination of high Stokes number and low resistance parameter (values to the left and above the "line" of points behind Figure 9, as indicated above Figure 15) can only be reached for $z_0 < 10^{-5}$ m, an unrealistically small value.

Combinations of low E_v and high $\hat{S}$, values to the right and under the points belonging to Figure 14, are only reached for $z_0 > 10^{-1}$ m. Such large values of z_0 correspond to bed forms with larger scales than megaripples. Since the generation of these large-scale bed forms is the subject of this study, the corresponding z_0 value cannot be used to predict them.

From (6) and (24) it can be seen that the ratio $E_v/\hat{S}$ decreases as ε increases. In Figure 15 this ratio is the "gradient" of the line of points. It is smallest for the line of points corresponding to the largest values of ε (Figures 13 and 14).

The collection of points in Figure 15 determine the possible combinations of E_v and $\hat{S}$ for a given (ε, z_0) combination in the North Sea. The specific value of E_v and $\hat{S}$ (within the collection) are, apart from the parameters already mentioned, determined by the local depth H and tidal velocity amplitude u_m. Therefore all four parameters (ε, z_0, H, and u_m) are needed to predict whether or not large-scale bed features will develop. However, ε and z_0 (parameterizations of the viscosity and the bottom roughness) almost completely determine what bed features will develop in case the bed is not flat.

From Figure 15 it can be observed that the area occupied by the points of Figures 9 and 12 (ε constant) is larger than the area enclosed by the points of Figures 11 and 13 or Figures 12 and 14 (z_0 constant). This leads to the conclusion that keeping ε constant and varying z_0 between its realistic limits allow for more variation than when ε is varied and z_0 is constant. Thus z_0 is the most sensitive parameter in this prediction. Consequently, when a prediction of the bed state is to be made, one should concentrate on an accurate estimation of this parameter.

Using overall values for ε and z_0 yields enough variation in Stokes number and resistance parameter to enable the prediction of patches of different patterns. Locally, the variation in ε and z_0 is large enough to account for the prediction of various bed features. These results justify a more detailed approach using locally determined values of z_0. If one aims to choose overall parameters ε and z_0 so that the result is closest to the observations, the best typical values are $\varepsilon = 0.5$ and $z_0 = 10^{-2}$ m.

6. Prediction of Sand Waves in the Southern Bight of the North Sea

In order to be able to confront the model with measured data, a slightly more detailed approach is chosen. In this detailed study, attention is paid only to sand waves for the following reason. It is generally accepted that sand waves are morphodynamic features generated as linear unstable modes by tides, whereas sand banks can have many other origins (e.g., storm generation, relicts, and nonlinear sand wave interactions [*Komarova and Newell*, 2000], or even different origins, as data analysis of *Knaapen et al.* [2001] has shown a new large-scale bed pattern). Therefore it is unclear what is learned by comparing prediction and observation of sand banks. This would be a different study than is performed here.

The study area is restricted to the southern bight of the North Sea, between 50° and 54°N, because for this area more detailed information is available (see Figure 2). The main difference between this application and the previous results is that the parameter z_0 is not assigned overall values but, using depth information, is estimated on a local level. Although

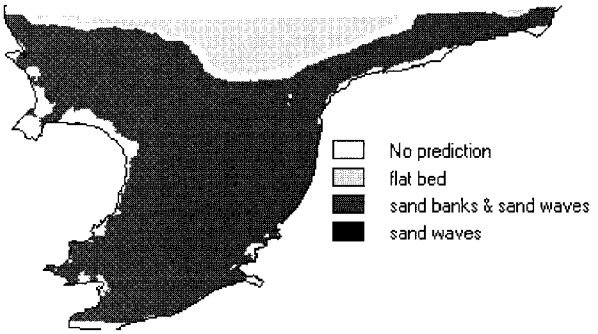

Figure 16. Prediction based on the diagram as in Figure 6 in the case of variable z_0 and $\varepsilon = 0.75$.

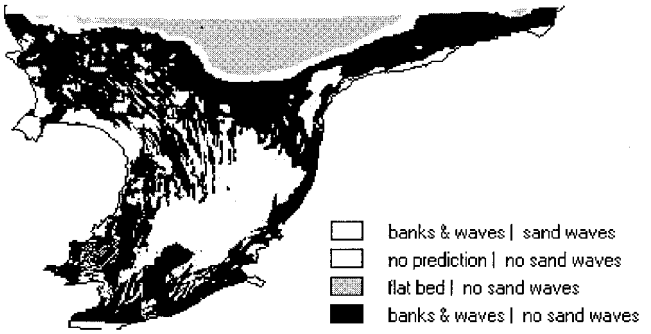

Figure 17. Predicted versus observed sand wave occurrence in the southern North Sea.

there are many objections that can undermine the validity of a such a simple z_0 concept in tidal motion, in this paper the local depth is used as a starting point to quantify the differences in horizontal roughness of the bed.

Experimental and theoretical research done so far [see, e.g., *Soulsby*, 1983, 1990, and references therein] has revealed different roughness heights for several types of bed composition and bed structure (ripples). Furthermore, it showed that the latter had the main impact on z_0. However, estimates on the distribution of z_0 over the entire North Sea are unknown. To deal with this, we performed an estimation procedure in which z_0 depends on the occurrence and size of small-scale megaripples on the bottom. To estimate the size of these megaripples, *Van Rijn* [1993] proposes the following for the height (Δ_r) and length (λ_r) as a function of the water depth H:

$$\Delta_r = \alpha H \qquad \lambda_r = \beta H, \tag{7}$$

in which α and β are dimensionless coefficients. *Tobias* [1989] used North Sea observations to arrive at the approximate values of $\alpha \cong 0.03$ and $\beta \cong 0.5$. These values relate to the megaripple regime [*Van Rijn*, 1993]. These ripples are the largest bed forms smaller than sand waves and are believed to be important to the formation of them [*Johnson et al*., 1981; *Houbolt*, 1968]. This concept is used here by relating the smaller-scale bed forms (megaripples) to the bed roughness. The ripple height Δ_r and length λ_r are used to estimate z_0 following the relation given by *Soulsby* [1983]:

$$z_0 = 2 \cdot \Delta_r \left(\frac{\Delta_r}{\lambda_r}\right)^{1.4}. \tag{8a}$$

Using (7), z_0 can also be expressed as a function of the water depth:

$$z_0 = 2\alpha^{2.4}\beta^{-1.4}H. \tag{8b}$$

The calculated values of z_0 at each point of the study area are introduced into the same model as in section 5. An overall value of $\varepsilon = 0.75$ was used. The results are shown in Figure 16.

In the entire southern bight of the North Sea a combination of tidal sand banks and sand waves is predicted. When the sea becomes deeper, the indication shifts to a flat bed, with a small strip in between for which no prediction is given. Note that this result is in agreement with the sand wave observations by *Stride* [1982] (see Figure 3) and with the earlier model results for the entire North Sea (cf. Figures 12 and 13).

The GIS was used to compare this prediction with the detailed information about sand wave occurrence, which was derived from *Rijks Geologische Dienst* [1984] and *Hydrographer of the Navy* [1992] and from *Van Alphen and Damoiseaux* [1989] (see Figure 2). The result of this combination is shown in Figure 17. It shows that almost all of the observed sand waves lie within the area in which sand wave occurrence is indeed predicted. In the northwest of the study area some observed features fall outside this area, and at a few locations sand waves are observed, although a flat bed had been predicted, but these are marginal effects only; the overall picture is similar. However, within the area of predicted sand wave occurrence, there are many locations in which they are not observed (dark shading in Figure 17).

The result of Figure 17 is quantified in Table 3, showing the distribution of the sand wave predictions over the areas with and without observed sand waves. It shows, once again, that the flat bed predictions are correct and that the observed sand waves lie in an area with the correct prediction.

A prediction is considered correct when (1) at a sand wave location sand waves are predicted while indeed occurring or (2) a flat bed prediction is given at a location without sand waves. The areas for which no prediction is given are not taken into account. From Table 3 it follows that the prediction is correct for 37% of the study area and incorrect for 54%, while no prediction is given for the remaining 9%. This confirms what can be concluded from Figure 17; that is, sand waves are predicted to occur at many more locations than they are observed. Nevertheless, almost all of the observed sand waves are included in the predicted area: 25/26 = 96%. Thus the "envelope" of the sand wave area has been predicted extremely well, but the model's ability to predict is much lower at the local level.

Table 3. Cross Tabulation of Observed and Predicted Sand Wave Areas

	No Prediction, %	Flat Bed, %	Banks and Waves, %	Total, %
Sand wave area	1	0	25	26
No sand wave area	8	12	54	74
Total	9	12	79	100

This leads to the conclusion that it is possible to estimate the values of z_0 adequately for an overall indication of the area where sand waves are likely to occur. Whether or not sand waves exist at a certain location is apparently determined by other factors than those included in the prediction model.

The viscosity variation parameter ε was kept constant because additional assumptions and data would be required to take its variation into account. A first attempt to vary ε, by relating it to wind wave data and allowing for maximum variation between its theoretical minimum and maximum, did not improve the results based on the variation of z_0 only.

By relating the level of zero intercept to the water depth it was implicitly assumed that z_0 is only determined by the smaller-scale bed topography. Subsequently, the size of these small-scale features is assumed to be a function of the water depth only. This rather simple parameterization was chosen for its simplicity (no additional data were required) and to test whether this model can be a starting point toward a more detailed prediction method. Equations (5)–(6) show that with z_0 being a linear function of the water depth H and ε assigned a global value the ratio $E_v/\hat{S}$ is constant. This substantially limits the range of possible $(E_v, \hat{S})$ combinations. In fact, the bundles in Figure 15, made up of separate points, reduce to a single line; there is only one degree of freedom left. Despite these limitations the model determined the transition from a flat bed to a sand wave area fairly well. Apparently, the gradient of the line $E_v/\hat{S}$ is determined accurately enough to predict this transition. The viscosity variation parameter ε was assigned an overall value. It can be shown that using any overall value of ε yields similar results.

The physical basis of *Hulscher*'s [1996] model is relatively simple because the model was meant to provide a first insight into the free behavior of the morphodynamic system. It seems obvious that such a model does not cover all possible factors associated with the development of large-scale rhythmic bed features. The results shown in this paper suggest that there may be other factors, not included in the model, that play a role in whether or not sand waves or tidal sand banks will develop at a certain location.

As can be seen from Section 3 and Figure 4, one of those possible factors is the type of bed material. Figure 2 shows that the sand wave patches become much more scattered near the English coast. This is also the area where moderate to large amounts of gravel are found. Figure 4 shows that sand waves do not occur when the bed contains moderate to large amounts of gravel.

To illustrate this, a cross-tabulation as in Table 3 was carried out, omitting the areas that contain more than 30% of gravel. The cross-tabulation was done for the area covered by the geological charts [*Rijks Geologische Dienst*, 1984; *Hydrographer of the Navy*, 1992] (see also section 2). This area covers only a part of the North Sea, but it is still large enough to yield reliable results. Of this area, 33% is covered with sand waves and 15% is dominated by gravel. The predictions are correct for 44% of the new area and incorrect for 49%, while there was no valid prediction for 7% of the area. In addition, note that in the gravelled areas the prediction (i.e., a flat bed) is also correct. This significantly improved accuracy of the prediction shows that the bed material is indeed important to the development of large-scale rhythmic features and should therefore be included in the model. A straightforward way to do this is to adopt an expression in which the level of zero intercept z_0 depends not only on the local depth but also on the bed material properties. The empirical expression used here, z_0 as a linear function of the depth, is too simple to be realistic. Also, including bed material properties requires additional data on sediment characteristics. With the data presently available, such an improved model could only be validated in a small part of the North Sea.

The critical bed shear stress is not accounted for in the predictions. Its existence would here imply that below a certain threshold value of the tidal velocity, no sediment transport occurs during the tidal cycle. An estimation of this threshold value near the bed [cf. *Komarova and Hulscher*, 2000] ($\tau_c \cong 0.8\ \mathrm{m\ s^{-2}}\, D$, where D is the grain diameter; so, for $D = 200$ μm, at a nonlinear friction formulation $\tau_c = c_D u_c|u_c|$ and $c_D = 0.0025$, we find $u_c \cong 0.25\ \mathrm{m\ s^{-1}}$) indicates that the tidal current amplitudes in the southern part of the North Sea largely exceed this threshold but that the threshold may play a more important role in the northern part. In the northern part it will drop the sediment transport to zero so that a flat bed would be predicted here, which is also observed. Note that this threshold can easily be incorporated into the model by predicting a flat bed whenever u_m drops below this threshold value.

7. Conclusions

The starting point of this study was the morphodynamic model presented by *Hulscher* [1996]. The underlying hypothesis is that large-scale bed features are free instabilities of the morphodynamic system. From this rather sophisticated model a parametric large-scale bed form prediction model was derived, based on the parameters depth, tidal velocity, level of zero intercept z_0, and a (eddy) viscosity variation parameter ε.

Several spatially constant values of the latter two parameters were used to make overall predictions for the entire North Sea. It was shown for the shallower southern bight of the North Sea that the range of possible values of ε and z_0 is large enough to let these parameters distinguish between the possible (combinations of) bed forms. When using spatially varying values for z_0, by relating z_0 to depth information, the area where sand waves occur in the southern part of the North Sea is predicted quite well. Both qualitatively and quantitatively the results showed that the model is able to predict the contours of the area in which sand waves can be expected. However, the model is unable to explain the smaller-scale variation within this area.

Furthermore, it is concluded that the prediction method, using variable z_0, is able to predict the contours of the area where sand waves can be expected, but that there must be other factors, not included in the model, that determine whether or not sand waves will develop at a certain location within that area. It is shown that one of those possible factors is the type of bed deposit. Although perhaps obvious, it was quantified that in the North Sea, sand waves only occur at locations where sand is the dominant bed material. Even small fractions of gravel and/or mud in the bed lead to the absence of sand waves. In general, this work confirms the validity of the bed form generation model of *Hulscher* [1996] and hence of the hypothesis that large-scale rhythmic bed features are free instabilities of the morphodynamic system.

Appendix A: Fitting the Coefficients E_v and $\hat{S}$

The two turbulence models are applied to horizontally uniform tidal flow, i.e., the inertial and Coriolis terms, as well as

secondary flow effects, are neglected. The tidal flow is driven by a pressure gradient, which oscillates at the tidal frequency σ and with amplitude $\partial P/\partial x$. The corresponding equation of motion becomes

$$0 = -\frac{1}{\rho}\frac{\partial P}{\partial x}\sin \sigma t + \frac{\partial}{\partial z}\left[\nu_t(z, t)\frac{\partial \tilde{u}}{\partial z}\right] \tag{A1}$$

in which ν_t is the eddy viscosity. The boundary conditions are

$$\begin{aligned} \tilde{u} &= 0, \qquad z = z_0, \\ \nu_t(z,t)\frac{\partial \tilde{u}}{\partial z} &= 0, \qquad z = H, \end{aligned} \tag{A2}$$

where z_0 is the level of zero intercept and H is assumed to be constant.

The bottom shear stress is usually expressed in terms of the depth-averaged velocity, via a nonlinear expression. To overcome this difficulty, the bed shear stress is expressed as

$$\tilde{\tau}_b = \rho\nu_t(z)\frac{\partial \tilde{u}}{\partial z} \equiv \rho \bar{u}_* \tilde{u}_* \tag{A3}$$

in which $\bar{u}_*$ is a time-averaged representative of the oscillating friction velocity $\tilde{u}_*$.

Assuming that the friction velocity oscillates with the tidal frequency σ (like the forcing pressure gradient) and that it has an amplitude $\hat{u}_*$, $\bar{u}_*$ can be determined from the requirement that the total energy loss due to the linearized friction is the same as that due to the nonlinear friction [see, e.g., *Zimmerman*, 1981]:

$$\bar{u}_* = \frac{8}{3\pi}\hat{u}_*. \tag{A4}$$

For time invariant eddy viscosity and in absence of inertia the tidal flow can be decomposed as follows:

$$\tilde{u}(z, t) = u(z)\sin \sigma t. \tag{A5}$$

Substitution of (13) into (9) leads to the following equation of motion:

$$0 = -\frac{1}{\rho}\frac{\partial P}{\partial x} + \frac{\partial}{\partial z}\left[\nu_t(z)\frac{\partial u}{\partial z}\right]. \tag{A6}$$

By integration of (14) using the upper boundary condition (10) and the lower as given in (11) the following expression is obtained:

$$\frac{1}{\rho}\frac{\partial P}{\partial x}H = \bar{u}_*\hat{u}_* = \frac{8}{3\pi}\hat{u}_*^2. \tag{A7}$$

By using the parabolic eddy viscosity distribution of (3), (14), the boundary conditions in (10) and (11), and the result of (12), the velocity profile $u(z)$ is found. Subsequently, the depth-averaged velocity $\bar{u}$ becomes

$$\bar{u} = \frac{\hat{u}_*}{\kappa}\left[\ln\left(\frac{H}{z_0}\right) - \frac{1}{\varepsilon} + \frac{1-\varepsilon}{\varepsilon}\ln\left(\frac{1-\varepsilon}{1-\varepsilon\dfrac{z_0}{H}}\right) + \frac{\varepsilon - 1}{\varepsilon^2}\ln(1-\varepsilon)\right], \tag{A8}$$

or $\bar{u} = \hat{u}_*\kappa^{-1}A$, where A represents the term in brackets.

The $A_v - S$ model of *Hulscher* [1996] uses a vertically constant eddy viscosity A_v and a partial slip condition at the bottom, in this context defined as

$$\bar{u}_*\hat{u}_* = Su, \qquad z = 0, \tag{A9}$$

in which S is the resistance parameter. The depth-averaged velocity according to this model is given by

$$\bar{u} = \hat{u}_*\bar{u}_*\left(\frac{H}{3A_v} + \frac{1}{S}\right). \tag{A10}$$

The models are matched at the following points.

1. The depth-averaged velocities must be equal. With (16) and (18) this leads to

$$\kappa\hat{u}_*\left(\frac{H}{3A_v} + \frac{1}{S}\right) = A. \tag{A11}$$

2. The depth-averaged eddy viscosities must be equal; averaging (3), this leads to

$$A_v = \kappa\hat{u}_* HB, \qquad B = \frac{3 - 2\varepsilon}{6}. \tag{A12}$$

Note that the condition of equal bed shear stress is inherently met by using the expressions of (11) and (17).

If the depth-averaged velocity $\bar{u}$ is known, from measurements or from a numerical model, this equation has to be rewritten in terms of this velocity u_m. With $u_m = \bar{u}$ and using (12) and (18) the friction velocity amplitude $\hat{u}_*$ can be expressed in u_m:

$$\hat{u}_* = \sqrt{\frac{3\pi}{8}\frac{u_m}{\left(\dfrac{H}{3A_v} + \dfrac{1}{S}\right)}}. \tag{A13}$$

Substitution of $\hat{u}_*$ into (20) yields

$$\left(\frac{H}{3A_v} + \frac{1}{S}\right)A_v^2 = (\kappa HB)^2\frac{3\pi}{8}u_m. \tag{A14}$$

Using the definitions of E_v and $\hat{S}$, (2) yields

$$\left(\frac{1}{3} + \frac{E_v}{\hat{S}}\right)E_v = \frac{2(\kappa B)^2}{H\sigma}\frac{3\pi}{8}u_m. \tag{A15}$$

A second expression for the relation between E_v and $\hat{S}$ is obtained by combining (12), (19), and (20):

$$\frac{E_v}{\hat{S}} = AB - \frac{1}{3}. \tag{A16}$$

Substitution of (24) into (23) yields explicit expressions for E_v and $\hat{S}$; see (5) and (6).

Acknowledgments. This work was begun within the project of the U.K. Ministry of Agriculture, Fisheries and Food (MAFF) under contract CSA3051-Offshore sand banks: Basic processes and effects on long-term coastal morphodynamics. After this, Suzanne Hulscher's part of this paper was carried out in the PACE project, within the framework of the EU-sponsored Marine Science and Technology Programme (MAST-III), under contract MAS3-CT95-0002 and supported by the Technology Foundation STW, the applied science division of NWO, and the technology programme of the Dutch Ministry of Economic Affairs. The authors wish to thank D. A. Roelvink for his cooperation during the MAFF project. R. Bijker and J. Wilkens are acknowledged for their guidance and work regarding the GIS, R.

Buijsrogge is acknowledged for his help with the figures, and H. de Vriend is acknowledged for his advice.

References

Bijker, R., J. Wilkens, and S. J. M. H. Hulscher, Sandwaves: Where and why, in *Proceedings of the Eighth International Offshore and Polar Engineering Conference*, vol. 2, pp. 153–158, Int. Soc. of Offshore and Polar Eng., Golden, Colo., 1998.

Boon, J. G., and H. Gerritsen, Modelling of suspended particulate matter (SPM) in the North Sea: A dedicated orthogonal boundary-fitted modelling approach (PROMISE), *Res. Rep. Z2025*, Delft Hydraul., Delft, Neth., 1997.

Directorate of Fisheries, *Atlas of the Seas Around the British Isles*, 100 pp., Minist. of Agric. Fish. and Food, London, 1981.

Dyer, K. R., and Huntley, D. A., The origin, classification and modelling of sand banks and ridges, *Cont. Shelf Res*., *19*, 1285–1330, 1999.

Engelund, F., Instability of erodible beds, *J. Fluid Mech*., *42*, 225–244, 1970.

Fenster, M. S., D. M. Fitzgerald, W. F. Bohlen, R. S. Lewis, and C. T. Baldwin, Stability of a giant sand wave field in eastern Long Island Sound, USA, *Mar. Geol*., *91*, 207–225, 1990.

Houbolt, J. J. H. C., Recent sediments in the southern bight of the North Sea, *Geol. Mijnbouw*, *47*, 245–273, 1968.

Hulscher, S. J. M. H., Tidal-induced large-scale regular bed form patterns in a three-dimensional shallow water model, *J. Geophys. Res*., *101*, 20,727–20,744, 1996.

Hulscher, S. J. M. H., H. E. De Swart, and H. J. De Vriend, The generation of offshore tidal sand banks and sand waves, *Cont. Shelf Res*., *13*, 1183–1204, 1993.

Huntley, D. A., J. M. Huthnance, M. B. Collins, C.-L. Liu, R. J. Nicholls, and C. Hewitson, Hydrodynamics and sediment dynamics of North Sea sand waves and sand banks, *Philos. Trans. R. Soc. London*, *Ser. A*, *343*, 461–474, 1993.

Huthnance, J., On one mechanism forming linear sand banks, *Estuarine Coastal Shelf Sci*., *14*, 79–99, 1982.

Hydrographer of the Navy, Spurn, East Anglia: Associated British Ports; Thames Estuary, Taunton, Engl., U. K., 1992.

Johnson, M. A., A. H. Stride, R. H. Belderson, and N. H. Kenyon, Predicted sand-wave formation and decay on a large offshore tidal-current sand-sheet, *Spec. Publ. Int. Assoc. Sedimentol*., *5*, 247–256, 1981.

Knaapen, M. A. F., S. J. M. H. Hulscher, H. J. DeVriend, and A. Stolk, A new type of sea bed waves, *Geophys. Res. Lett*., *28*, 1323–1326, 2001.

Komarova, N. L., and S. J. M. H. Hulscher, Linear instability mechanisms for sand wave formation, *J. Fluid Dyn*., *413*, 219–246, 2000.

Komarova, N. L., and A. C. Newell, Nonlinear dynamics of sand banks and sand waves, *J. Fluid Dyn*., *415*, 285–321, 2000.

Langhorne, D. N., Offshore engineering and navigational problems: The relevance of sand wave research, 21 pp., Soc. Underwater Technol., London, 1978.

Rijks Geologische Dienst, Geological charts of the North Sea: Indefatigable, Flemish Bight, Ostend, Haarlem, Netherlands, 1984.

Soulsby, R. L., The bottom boundary layer of shelf seas, in *Physical Oceanography of Coastal and Shelf Seas*, edited by B. Johns, pp. 189–266, Elsevier Sci., New York, 1983.

Soulsby, R. L., Tidal-current boundary layers, in *The Sea*, vol. 9, *Ocean Engineering Science*, edited by B. le Méhauté and D. M. Hanes, pp. 523–566. John Wiley, 1990.

Stride, A. H. (Ed.), Offshore tidal sands: Processes and deposits, 222 pp., Chapman and Hall, New York, 1982.

Ten Brummelhuis, P. G. J., H. Gerritsen, and T. Van der Kaay, Sensitivity analysis and calibration of the orthogonal boundary-fitted coordinate model PROMISE for tidal flow: The use of adjoint modelling techniques, *Res. Rep. Z2025*, Delft Hydraul., Delft, Neth., 1997.

Terwindt, J. H. J., Sand waves in the southern bight of the North Sea, *Mar. Geol*., *10*, 51–67, 1971.

Tobias, C. J., Morphology of sand waves in relation to current, sediment and wave data along the Eurogeul, North Sea; *Rep. GEOPRO 1989.01*, Dep. of Phys. Geogr., Univ. of Utrecht, Utrecht, Neth., 1989.

Van Alphen, J. S. L. J., and M. A. Damoiseaux, A geomorphological map of the Dutch shoreface and adjacent part of the continental shelf, *Geol. Mijnbouw*, *68*, 433–444, 1989.

Van Dijk, R., and R. Plieger, Definitieve versie ZUNOWAK model (in Dutch), *Rep. GWAO-88.381*, Rijkswaterstaat, dienst Getijdewateren, The Hague, Netherlands, 1988.

Van Rijn, L. C., *Principles of Sediment Transport in Rivers, Estuaries and Coastal Seas*, Aqua, Amsterdam, 1993.

Whitehouse, R., N. Beech, S. J. M. H. Hulscher, and D. Huntley, Understanding the behaviour and engineering significance of offshore and coastal sand banks, paper presented at 33rd Annual MAFF Conference of River and Coastal Engineers, Minist. of Agric. Fish. and Food, Keele, Engl., U. K., 1998.

Zimmerman, J. T. F., On the Lorentz linearization of a quadratically damped forced oscillator, *Phys. Lett. A*, *89*, 123–124, 1981.

S. J. M. H. Hulscher and G. M. van den Brink, Department of Civil Engineering, University of Twente, P.O. Box 217, 7500 19E Enschede, Netherlands. (s.j.m.h.hulscher@sms.utwente.nl)

(Received March 30, 1999; revised December 4, 2000;
accepted December 29, 2000.)